Journal of Power Sources 190 (2009) 241–251

Contents lists available at ScienceDirect

Journal of Power Sources

journal homepage: www.elsevier.com/locate/jpowsour

Pd and Pt–Ru anode electrocatalysts supported on multi-walled carbon nanotubes and their use in passive and active direct alcohol fuel cells with an anion-exchange membrane (alcohol = methanol, ethanol, glycerol)

Valentina Bambagioni [a], Claudio Bianchini [a,*], Andrea Marchionni [a], Jonathan Filippi [a], Francesco Vizza [a,*], Jacques Teddy [b], Philippe Serp [b], Mohammad Zhiani [a,1]

[a] Istituto di Chimica dei Composti Organometallici (ICCOM-CNR), Via Madonna del Piano 10, 50019 Sesto Fiorentino, Italy
[b] Laboratoire de Chimie de Coordination UPR8241 CNRS, composante ENSIACET, 118 Route de Narbonne, F-31077 Toulouse Cedex, France

ARTICLE INFO

Article history:
Received 25 September 2008
Received in revised form 9 December 2008
Accepted 18 January 2009
Available online 23 February 2009

Keywords:
Direct alcohol fuel cell
Anion-exchange membrane
Alcohol electro-oxidation
Carbon nanotubes
Palladium catalyst
Platinum–ruthenium catalyst

ABSTRACT

Palladium and platinum–ruthenium nanoparticles supported on multi-walled carbon nanotubes (MWCNT) are prepared by the impregnation-reduction procedure. The materials obtained, *Pd/MWCNT* and *Pt–Ru/MWCNT*, are characterized by TEM, ICP-AES and XRPD. Electrodes coated with *Pd/MWCNT* are scrutinized for the oxidation of methanol, ethanol or glycerol in 2 M KOH solution in half cells. The catalyst is very active for the oxidation of all alcohols, with glycerol providing the best performance in terms of specific current density and ethanol showing the lowest onset potential. Membrane-electrode assemblies have been fabricated using *Pd/MWCNT* anodes, commercial cathodes and anion-exchange membrane and evaluated in both single passive and active direct alcohol fuel cells fed with aqueous solutions of 10 wt.% methanol, 10 wt.% ethanol or 5 wt.% glycerol. *Pd/MWCNT* exhibits unrivalled activity as anode electrocatalyst for alcohol oxidation. The analysis of the anode exhausts shows that ethanol is selectively oxidized to acetic acid, detected as acetate ion in the alkaline media of the reaction, while methanol yields carbonate and formate. A much wider product distribution, including glycolate, glycerate, tartronate, oxalate, formate and carbonate, is obtained from the oxidation of glycerol. The results obtained with *Pt–Ru/MWCNT* anodes in acid media are largely inferior to those provided by *Pd/MWCNT* electrodes in alkaline media.

1. Introduction

Primary alcohols, with a higher molecular weight than methanol, and polyalcohols are arousing major interest as fuels in *direct alcohol fuel cells* (DAFC) for various reasons, among which there are their low toxicity, high boiling point, high specific energy and the capacity of some of them to be renewable [1–4]. Included in this group are ethanol and glycerol. The former can be massively produced from biomass feedstocks originating from agriculture (first-generation bio-ethanol), and forestry and urban residues (second-generation bio-ethanol). The latter is a by-product of biodiesel production and, as such, is inexpensive and largely available. Both alcohols, however, are difficult to oxidize on platinum or platinum alloys supported on carbon blacks that constitute the most common catalysts to realize anodes for DAFCs [1–5]. In particular, no known anode catalyst based on platinum has demonstrated the capacity to produce acceptable power densities in either a *direct ethanol fuel cell* (DEFC) or a *direct glycerol fuel cell* (DGFC) even at high metal loading [1–4,6]. The overall efficiency of Pt-based electrocatalysts suffers the consequences of effective catalyst poisoning by CO that is an intermediate of the oxidation of any alcohol [1–4,7]. Notable efforts are therefore being carried out to design new catalytic structures for DAFC anodes that do not contain platinum or contain tiny amounts of this too rare metal and, most of all, are able to oxidize primary and secondary alcohols with fast kinetics and tolerable deactivation. Palladium has recently aroused notable interest in electrocatalysis as it is more abundant in nature, hence less expensive, than platinum, and has the capacity to promote the oxidation of several alcohols, including ethanol and glycerol in alkaline media, with remarkable electrochemical stability [3,8–11].

In addition to platinum-free metal catalysts, increasing research efforts are being directed to develop conductive supports, alternative to carbon black, in an attempt of improving the dispersion, activation and stability of the metal particles on the carbon surface as well as increasing the electroconductivity [12].

A large variety of conductive materials has been used to support Pd nanoparticles for use in electrocatalysis, these include carbon blacks like Vulcan XC-72, alone [13] or in combination with either

* Corresponding authors. Tel.: +39 0555225280; fax: +39 0555225203.
E-mail address: claudio.bianchini@iccom.cnr.it (C. Bianchini).
[1] Present address: Department of Physical Chemistry, Faculty of Chemistry, Isfahan University of Technology, Isfahan, Iran.

0378-7753/$ – see front matter © 2009 Elsevier B.V. All rights reserved.
doi:10.1016/j.jpowsour.2009.01.044

nanocrystalline metal oxides (NiO, CeO_2, Co_3O_4, Mn_3O_4) [8–11,14] or tungsten carbide nanocrystals [15], carbon microspheres [16], coin-like hollow carbons [17], ultrahigh-surface hollow carbon spheres [18], carbonized porous anodic alumina [9], carbonized TiO_2 nanotubes [19], multi-walled carbon nanotubes [20] and activated carbon nanofibers [20]. To the best of our knowledge, however, no report has ever appeared in the relevant literature where a Pd catalyst is used in a real DAFC, all the known studies being limited to alcohol oxidation in half cells [8–11,13–20].

In this paper, we describe the synthesis and characterization of a new Pd-electrocatalyst supported on MWCNTs and its use to manufacture anodes for the oxidation of methanol, ethanol or glycerol in either passive or active DAFCs equipped with an anion-exchange membrane. For comparative purposes, we have also prepared and characterized a Pt–Ru catalyst supported on the same MWCNTs and used in a *direct methanol fuel cell* (DMFC) in conjunction with a proton-exchange membrane.

2. Experimental

2.1. Materials and product analysis

All manipulations, except as stated otherwise, were routinely performed under argon or nitrogen atmosphere using standard airless technique. Aqueous solutions were freshly prepared with doubly distilled-deionized water. The MWCNTs were prepared by catalytic CVD and were treated with (i) sulfuric acid (H_2SO_4 50% (v:v) for 14 h) to clean the surface and purify the tubes from catalyst residue (MWCNTs purity >97%, 3 wt.% remaining iron particles encapsulated in MWCNTs) and (ii) nitric acid (HNO_3 65%, 120 °C, 8 h) to activate the surface for chemical bonding with the organometallic precursors via the formation of carboxylic surface groups (–COOH) [21]. The atomic oxygen percentage as determined by XPS after nitric acid treatment was ca. 7%. The MWCNT-supported Pd and Pt–Ru materials were prepared from the following organometallic precursors: dimethylcyclooctadiene platinum [$Pt(CH_3)_2(COD)$], cyclooctadiene cyclooctatriene ruthenium [Ru(COD)(COT)], and tris(dibenzylideneacetone)dipalladium [$Pd_2(dba)_3$]. The latter two complexes were purchased from NanoMePS (Toulouse, France), while [$Pt(CH_3)_2(COD)$] was prepared according to a reported procedure [22]. The alkaline solid electrolyte used in both passive and active DAFCs was a Tokuyama anion-exchange membrane A-006 (OH-type) obtained from Tokuyama Corporation. The cation-exchange membrane was a Nafion® 117 (Du Pont) material purchased from Aldrich. The cathodes were provided by ACTA S.p.A. (Fe-Co-based Hypermec™ K-14). The quantitative analysis of the FC cell exhausts was obtained by $^{13}C\{^1H\}$ NMR spectroscopy using a Bruker Avance DRX-400 instrument with the chemical shifts relative to external TMS. The calibration curves for the quantitative analysis were obtained using authentic samples of the various products in the appropriate range of concentrations, using 1,4-dioxane as internal standard. Ionic chromatography (IC) was also used to identify the oxidation products (Metrohm 761 Compact instrument equipped with a Metrosep Organic Acids column).

2.2. Catalyst preparation

2.2.1. Pd/MWCNT

To a suspension of 1 g of MWCNTs in a 250 mL flask containing 50 mL of THF wad added a solution of [$Pd_2(dba)_3$] (0.25 g) in 50 mL of THF. A condenser was connected to the flask and the resulting mixture was magnetically stirred at room temperature for 3 days. The solid product was filtered off and dried under vacuum, then it was grounded and treated in an oven under 100 sccm (Standard Cubic Centimeters per Minute) of hydrogen flow for 4 h at 200 °C. The final material was collected and stored under argon.

Pd content: 3.8 wt.%

2.2.2. Pt–Ru/MWCNT

Into a 250 mL flask containing 65 mL of toluene de-aerated with argon were introduced 2 g of MWCNTs. After sonication under argon for 1 h were added 1.0 g of [Ru(COD)(COT)] and 0.7 g of [$Pt(CH_3)_2(COD)$]. Hydrogen gas was bubbled into this solution at 110 °C for 1 day. After cooling to room temperature, toluene was evaporated from the resulting yellow solution under vacuum. The solid residue was calcined at 300 °C under air for 3 h, then it was treated with a hydrogen flow (100 sccm) at 300 °C for 2 h.

Metal content: Pt 4.5 wt.%; Ru 2.5 wt.%.

2.3. Catalyst characterization

The TEM micrographs have been recorded with a JEOL JEM 1011 microscope operating at 100 kV. The metal content in all catalysts was determined by inductively coupled plasma atomic emission spectroscopy (ICP-AES) with a Intrepid Iris instrument (Thermo Elemental). Powder X-ray diffraction (XRPD) spectra were acquired at room temperature with a Bruker D8-Advance diffractometer, employing Cu Kα radiation (λ = 1.5418 Å) in the range between 2.5 and 80.0° and using an acquisition step of 0.030° per second.

2.4. Electrochemical measurements

2.4.1. Ink preparation for the CV study

2.4.1.1. Pd/MWCNT. A portion of *Pd/MWCNT* (about 45 mg) was introduced into a 5 mL high-density polyethylene container together with 1.01 g of water, 65 mg of KOH (99.99% Sigma–Aldrich), 0.50 g of absolute ethanol (99.8% Fluka) and 0.37 g of 5% Nafion® ion-exchange resin in alcohol solution (Sigma–Aldrich). The resulting suspension was sonicated for 30 min with a Branson 3200 bath. Each suspension was freshly prepared just before carrying out the experiment scheduled. The metal loading on each glassy carbon electrode (*vide infra*) was determined by weighting the amount of ink deposited on the glassy carbon disk.

2.4.1.2. Pt–Ru/MWCNT. The procedure was analogous to that described above except for the absence of KOH.

2.4.2. Apparatus for cyclic voltammetry studies

The cell used for the cyclic voltammetry (CV) experiments was a Kelef cylinder with a 7.2 mm inner diameter and a 50 mm outer diameter. The inner volume of the cell was about 1 mL. The working electrode, Glassy Carbon (Sigradur® G) (0.867 cm^2), covered by the catalyst, was housed in a cavity at the top end of the cylinder, and the counter electrode was a gold disc placed at the bottom end. The solution contained in a Pyrex flask was previously de-aerated by bubbling N_2, and then flushed into the cell by a pressure as low as 0.3 bar of N_2. The miniaturized reference electrode, $Ag/AgCl/KCl_{sat}$, was placed on the outlet tubing. This allocation allows one to avoid contamination and at the same time is sufficiently close to the working electrode to reduce the uncompensated resistance. All CV studies were carried out using a Parstat 2277 potentiostat-galvanostat (Princeton Applied Research).

2.4.3. Passive DAFC

The home-made, oxygen-breathing DAFC used to evaluate the electrochemical performance of the *Pd/MWCNT* anodes, in conjunction with the Tokuyama A-006 anion-exchange membrane and Fe-Co Hypermec™ cathodes, is shown in Fig. 1. The device was realized with *plexiglas* and the electricity collectors were plated with gold. The volume of the anode compartment was ca. 20–25 mL for

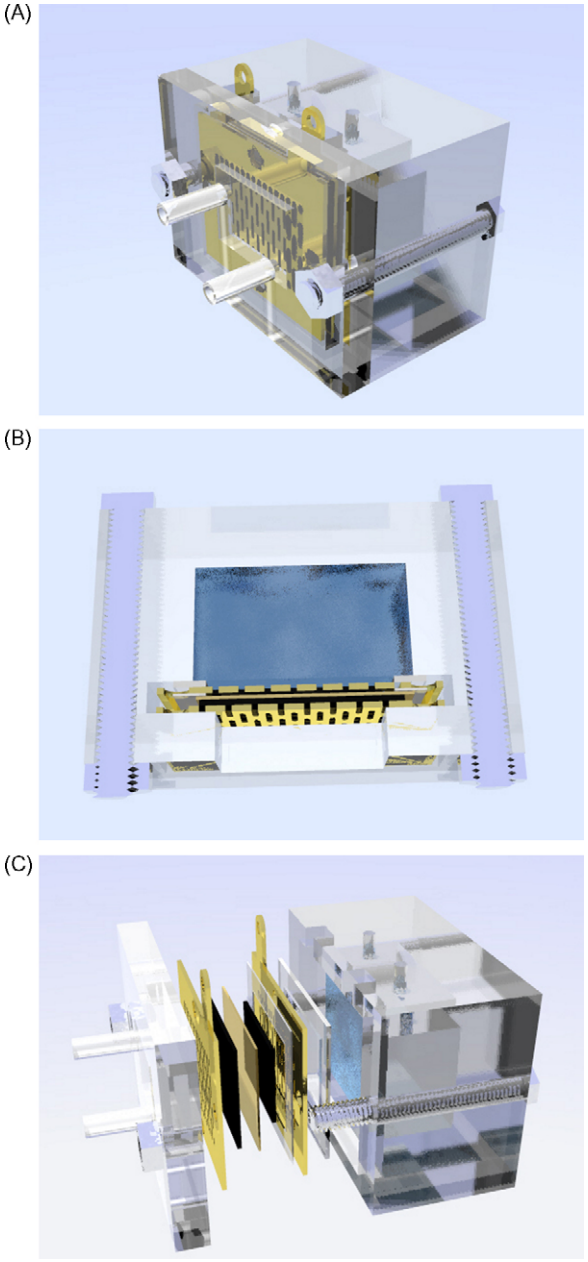

Fig. 1. The home-made oxygen-breathing DAFC used in this work. (A) Complete view. (B) Top view showing the anode compartment. (C) Exploded view showing the MEA.

an actual fuel solution of 13–15 mL. The anode was realized with a 5.13 cm^2 nickel foam plate onto which was deposited the appropriate amount of a dense catalytic ink. This was prepared by dispersing the solid catalyst (*Pd/MWCNT*) in the minimum amount of water with no need of a binder. The cathode (catalyzed carbon cloth) was provided by ACTA S.p.A. The membrane-electrode assembly (MEA) was obtained by mechanically pressing anode, cathode and membrane, while silicone–rubber gaskets were employed to seal the system.

In order to avoid any possible contamination of the alkaline anode solution by carbonate ions formed upon reaction with atmospheric CO_2, the DAFCs were positioned inside a home-made plexiglass dry-box where the anode compartment was maintained all the way under a static nitrogen atmosphere, while the cathode was exposed to either air or an oxygen flow.

The cell performance was evaluated with an ARBIN BT-2000 5A-4 channels instrument.

2.4.4. Active DAFC

The active DAFC were purchased from Scribner-Associates (USA) (25 cm^2 fuel cell fixture) and were modified in our laboratory with gold-plated current collectors and titanium end plates to tolerate the alkaline conditions used in this work to evaluate the performance of the *Pd/MWCNT*-catalyzed anode. The MEA was fabricated by mechanically pressing anode, Hypermec™ cathode and Tokuyama A006 membrane. A dense anode ink was prepared by mixing the powdered catalyst with a 5–10 wt.% aqueous dispersion of PTFE. As a general procedure, an identical amount of the resulting paste was spread onto two identical Ni-foam plates. One of these was used almost immediately to fabricate the MEA, the other was dried until constant weight for the quantitative determination of the Pd loading that was, in all cases, ca. 1 mg cm^{-2}. The effective electrode area was 5 cm^2. The fuel (water solutions containing 10 wt.% methanol, 10 wt.% ethanol or 5 wt.% glycerol in 2 M KOH) was delivered to the anode at 4 mL min^{-1} by a micropump, while the oxygen flow was regulated at 200 mL min^{-1}.

The entry temperatures of the fuel and of the oxygen gas were regulated at the desired temperature and the effective cell temperature under working conditions was determined by an appropriate sensor positioned inside the end plate at the cathode side.

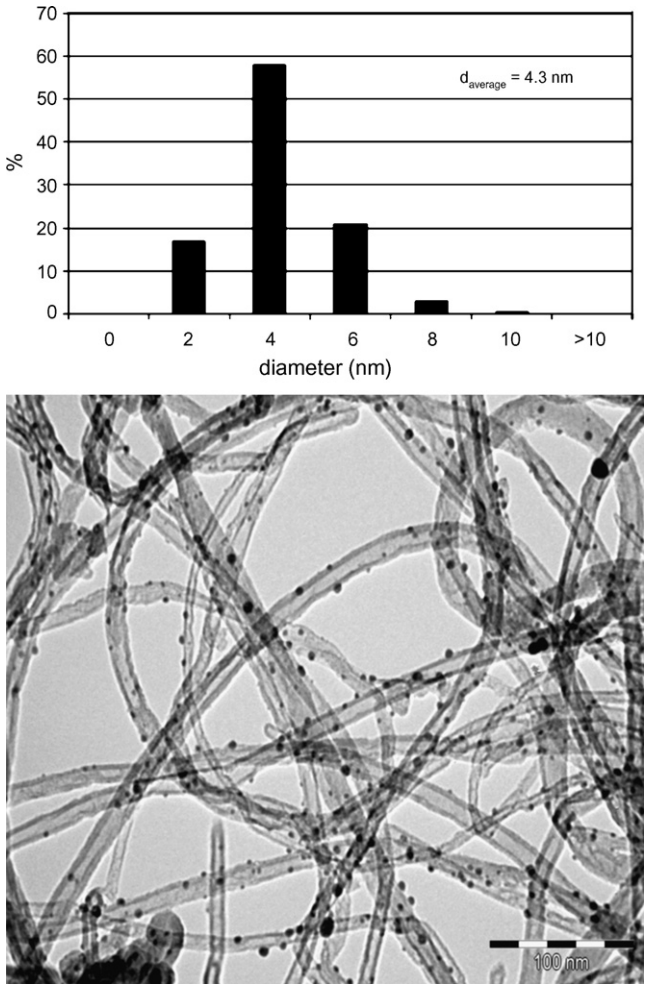

Fig. 2. TEM micrographs of *Pd/MWCNT* (scale bar: 100 nm) and histogram of particle distribution vs. diameter. Average size reported.

Except for the use of aluminum end plates, the DMFC employed to study the performance of the *Pt–Ru/MWCNT*-catalyzed anode was identical with that used in alkaline media. The MEA for this cell was made by hot-pressing a Nafion® 117 membrane together with an anode sheet and a cathode sheet. The anode sheet was carbon cloth (5 cm^2) painted with an ink made by dispersing the catalyst in a 25 wt.% Nafion® solution in alcohol. The cathode sheet was carbon cloth with a commercial Pt/C (30 wt.% metal) catalyst (E-TEK) dispersed in the same Nafion® binder. The catalyst loading at the anode and cathode was 0.7 and 2 mg cm^{-2}, respectively. Methanol was delivered at 1.5 mL min^{-1}, while the oxygen flow was 200 mL min^{-1}.

All electrochemical measurements were carried out using an 850e Integrated PEM Fuel cell Station by Scribner-Associates (USA).

3. Results and discussion

3.1. Catalyst characterization

3.1.1. TEM micrographs

The TEM analysis *of Pd/MWCNT* showed a rather narrow distribution of the metal particle size, with an overall mean diameter of 4.3 nm (Fig. 2). As shown by a selected micrograph (Fig. 2), the Pd nanoparticles were well dispersed on the surface of the MWCNTs with a few large particles (8–12 nm) on some tubes, which may be due to the aggregate effect caused by a lower amount of carboxylic acid groups on their surface [20,21].

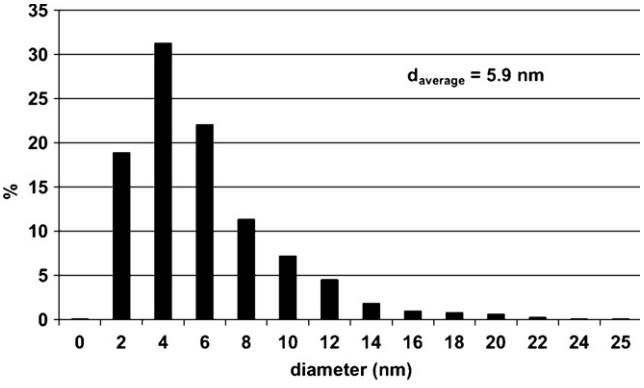

Fig. 3. TEM micrographs of *Pt–Ru/MWCNT* (scale bar: 50 nm) and histogram of particle distribution vs. diameter. Average size reported.

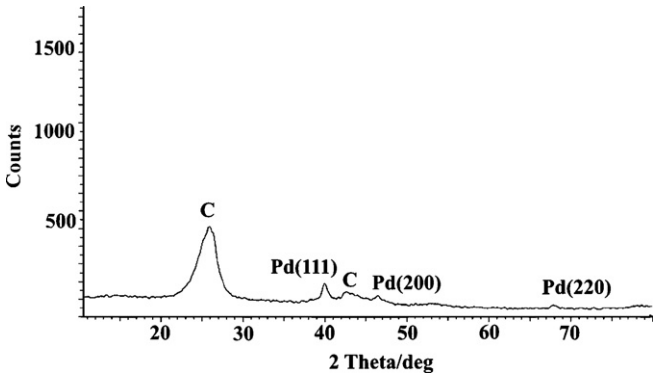

Fig. 4. XRPD pattern of *Pd/MWCNT*.

The metal particles in *Pt–Ru/MWCNT* were significantly larger (5.9_{av} nm), and less dispersed as well as less uniformly distributed on the MWCNT surface than in *Pd/MWCNT* (Fig. 3). In particular, one may notice an accentuated concentration of metal particles, which may be due to the higher metal loading in *Pt–Ru/MWCNT*.

3.1.2. XRPD analysis

The structure of *Pd/MWCNT* was investigated by XRPD. Fig. 4 shows the corresponding pattern where the diffraction peaks at the Bragg angles of 40.10°, 46.40° and 68.08° can be readily attributed to the (1 1 1), (2 0 0) and (2 2 0) facets of fcc Pd crystals [23,24], while the peaks at ca. 25° and 44° are typical of the hexagonal graphite structure of the carbon support [20].

The low intensity and broadness of the Pd peaks are consistent with the low metal loading as well as the high dispersion of the metal particles. The XRPD diagram of *Pt–Ru/MWCNT* is shown in Fig. 5. In addition to the peaks of the carbon support, the diagram displays the characteristic patterns of a Pt–Ru aggregate with a relatively high Ru content [25–29]. In particular, diffraction peaks could be indexed to the (1 1 1) (40.09°), (2 0 0) (46.56°), (2 2 0) (67.93°), (3 1 1) (82.10°), (2 2 2) (86.5°) planes of a Pt-rich fcc phase. For Ru nanoparticles (hexagonal), the diffraction peaks could be indexed to the (1 0 0) (38.60°), (1 0 1) (43.88°), (1 1 0) (68.48°) and (1 0 3) (78.04°) planes. Since all peaks were slightly shifted to higher 2θ values as compared to the separated elements, one cannot disregard the presence of a Pt–Ru alloy [25–27].

3.2. Electrochemical studies

3.2.1. Electrochemical characterization of Pd/MWCNT in KOH solution

The CV behaviour of *Pd/MWCNT* was preliminarily investigated in 2 M KOH solution. The corresponding cyclic voltammogram after

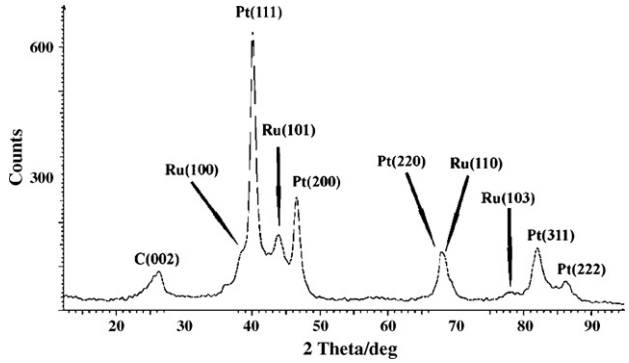

Fig. 5. XRPD pattern of *Pt–Ru/MWCNT*.

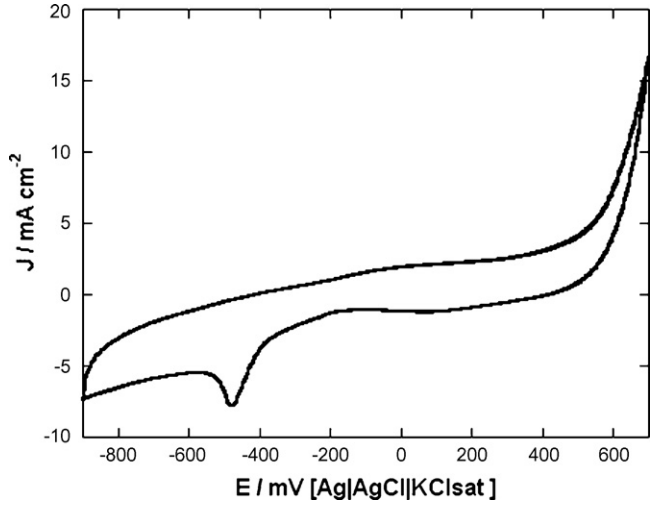

Fig. 6. Cyclic voltammogram of *Pd/MWCNT* (at the fifth cycle) in 2 M KOH solution. Pd loading 17 μg cm^{-2}. Scan rate: 50 mV s^{-1}.

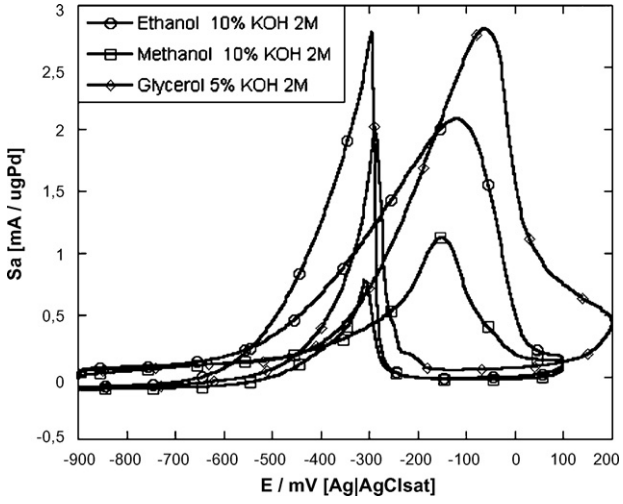

Fig. 7. Cyclic voltammograms (at the fifth cycle) of methanol, ethanol and glycerol oxidation on a *Pd/MWCNT* electrode in 2 M KOH solution. Pd loading: 17 μg cm^{-2}. Scan rate: 50 mV s^{-1}.

the fifth cycle is reported in Fig. 6; the forward scan showed a very broad oxidation wave starting at ca. −0.2 V, while a much narrower and more intense reduction peak was observed in the reverse scan with an onset potential of ca. −0.25 V with a peak at −0.47 V.

The position and shape of this reduction wave are consistent with the reduction of nanostructured Pd^{II} species, either PdO or $Pd(OH)_2$. Indeed, in the range of potential investigated, the formation of Pd^{IV} species is to be ruled out [30–33]. Previous CV studies of electrodes coated with either PdO or nanostructured Pd in NaOH solution agree to consider the redox chemistry of these species as a quite complex process due to the number of possible oxide/hydrous or oxide/hydroxyl surface species [30,34], which would explain the broad shape of the reduction wave.

3.2.2. Electrochemical oxidation of methanol, ethanol and glycerol on Pd/MWCNT in half cells

The electrochemical activity of *Pd/MWCNT* for methanol, ethanol and glycerol oxidation was investigated by CV at room temperature in deoxygenated 2 M KOH solutions. A series of cyclic voltammograms recorded at KOH concentrations spanning from 0.5 to 4 M showed the generation of the highest current densities in the range 1–1.5 M KOH. However all the following electrochemical studies, either in half cells or in monoplanar cells, were carried out using a 2 M KOH solution to keep the OH^- concentration as constant as possible along all over the experiment. Indeed, the oxidation of alcohols in alkaline media consumes OH^- groups, irrespective of the oxidation level of the substrate (*vide infra*) [6,35,36]. All the CV measurements were performed at a sweep rate of 50 mV s^{-1} on solutions containing 10 wt.% methanol, 10 wt.% ethanol or 5 wt.% glycerol using glassy carbon electrodes with a Pd loading between 16 and 17 μg cm^{-2} (Fig. 7). Higher alcohol concentrations, although yielding higher current densities, were not considered for minimizing the alcohol cross-over in the DAFCs. Indeed, it is generally found that at concentrations higher than 10 wt.%, the alcohol cross-over may become relevant for most polymer ion-exchange membranes [35,34]. This would result in increased cell overvoltage and also in decreased efficiency due to fuel loss by evaporation from the cathode compartment.

Relevant electrochemical parameters such as peak current density (J_p), specific peak current density (Sa_p), forward anodic peak potential (V_p) and Tafel slopes, together with the electronic transfer coefficient α, are given in Table 1 for all fuels investigated.

The catalyst was active for the oxidation reaction of all alcohols investigated. In terms of peak current density, glycerol provided the best performance out of the three alcohols investigated in spite of its lower concentration, yet ethanol showed the lowest onset potential (−0.75 V vs. > −0.60 for glycerol). The worst results were obtained with methanol, especially in terms of current density and oxidation overpotential.

Since the peak back current decreased with increasing the anodic limit (from −0.1 to 0.6 V) for all alcohols, one may reasonably conclude that the backward scan peaks are compatible with the oxidation of both freshly chemisorbed substrate and residual adsorbed species [26]. The less marked decrease of the backward scan peak observed for ethanol suggests the formation of more weakly adsorbed species as compared to those originated by methanol and glycerol (*vide infra*).

From a perusal of the literature and considering the very low Pd loading (16–17 μg cm^{-2}), one may readily realize that *Pd/MWCNT* can be classified among the most active electrocatalysts ever reported for the oxidation of alcohols in half cells, especially for ethanol and glycerol. Analogous results, in terms of onset potential and Jp for the oxidation of the present alcohols, have been reported by Shen et al. for a family of nanostructured Pd-electrocatalysts, which includes Pd/C (C = Vulcan XC-72 [10]), oxide-promoted Pd/C (oxide = CeO_2, NiO, Co_3O_4, Mn_3O_4 [11], and Pd/CPAA (CPAA = carbonized and pulverized anodic alumina) [9]. However, the Pd loading on the Shen's anodes, being signif-

Table 1
Relevant electrochemical parameters for the methanol, ethanol and glycerol oxidation reactions on a Pd/MWCNT electrode[a].

Substrate	J_p (mA cm^{-2})	Sa_p (mA μg Pd^{-1})	V_p[b] (V)	V_{onset} (V)	Tafel slope (mV dec^{-1})
Methanol	19.4	1.1	−0.15	−0.55	282 (α 0.21)
Ethanol	35.1	2.1	−0.12	−0.75	249 (α 0.24)
Glycerol	53.7	2.8	−0.08	−0.60	–

[a] Average values for at least three measurements.
[b] Versus $Ag/AgCl/KCl_{sat}$.

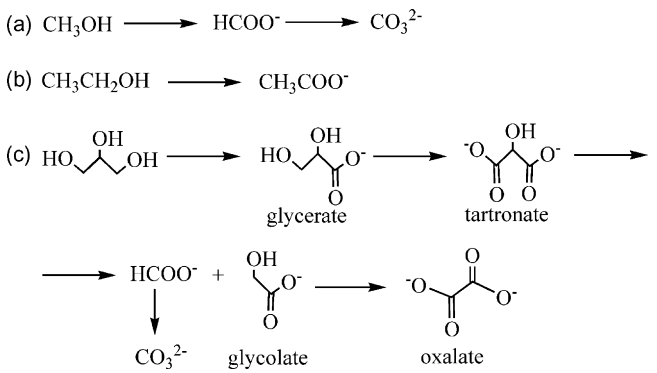

Scheme 1. Products obtained by electro-oxidation of (a) methanol; (b) ethanol; and (c) glycerol on *Pd*/*MWCNT*.

icantly higher than that in the present *Pd*/*MWCNT* catalyst (300 vs. 17 $\mu g\,cm^{-2}$), ultimately yields Sa_p values lower by ca. an order of magnitude, irrespective of the alcohol, even for the best oxide-supported Pd/C catalyst [9].

The larger dispersion of the metal particles in *Pd*/*MWCNT* than in Pd/C, oxide-promoted Pd/C or Pd/CPAA (3.8_{av} vs. 7–10 nm [9,10]) and the intrinsic properties of the MWCNT support (different macro- and meso-structure and higher electroconductivity and alcohol permeability as compared to a carbon black) may well account for the remarkable activity of the present catalyst. The effect of the carbon support on the activity of Pd-electrocatalysts for ethanol oxidation in alkaline media has been previously investigated by Shen et al. for Vulcan XC-72, MWCNTs and activated carbon fibers [20]. It was found that, at comparable metal loading, the MWCNT-supported catalyst gives improved performance in terms of both peak current density and electrochemical stability. On the other hand, a reliable comparison between the MWCNT-supported Pd catalyst described by Shen [9] and the present one is again precluded by the largely different Pd loadings (200 $\mu g\,cm^{-2}$ in the former for a J_p of 25 $mA\,cm^{-2}$; 17 $\mu g\,cm^{-2}$ in the latter for a J_p of 35.1 $mA\,cm^{-2}$), which apparently makes the *Pd*/*MWCNT* system twenty times more active for ethanol oxidation in terms of specific current density.

Tafel plots for methanol and ethanol oxidation reactions on the *Pd*/*MWCNT* electrode were obtained at a scan rate of 5 $mV\,s^{-1}$ in the potential interval from −0.5 to −0.4 V. The two values for the Tafel slopes and of the α coefficients (Table 1) are quite comparable with each other, yet they are significantly higher than those generally observed for nanostructured Pd catalysts supported on carbon black (ca. 190 $mV\,dec^{-1}$) [8,10]. The almost identical Tafel slopes for the oxidation of methanol and ethanol indicate the same reaction mechanism, while the α parameters of 0.21 and 0.24 are consistent with an electrochemical rate limiting step for the oxidation reaction of both alcohols. As for the absolute values of the Tafel slopes, the high values observed are in line with porous high surface area electrodes [8,37]. On such electrodes the charge transfer region is very narrow and mass transport interferences may be very important. Moreover, the oxidation of alcohols, especially of polyalcohols, can be mechanistically complicated by the occurrence of parallel steps (Scheme 1). This is certainly the case of the glycerol oxidation reaction on the *Pd*/*MWCNT* electrode for which no linear dependence of log J vs. overpotential was actually observed (*vide infra*).

The performance stability of the *Pd*/*MWCNT* electrocatalyst for methanol, ethanol and glycerol oxidation was investigated by chronopotentiometry. Steady state measurements were carried out by a constant current density polarization of 3.46 $mA\,cm^{-2}$ (Fig. 8).

As shown by the chronopotentiometric traces, the steady-state oxidation of ethanol was quite stable with negligible potential oscillation, indicative of no strongly adsorbed species on the catalyst surface.

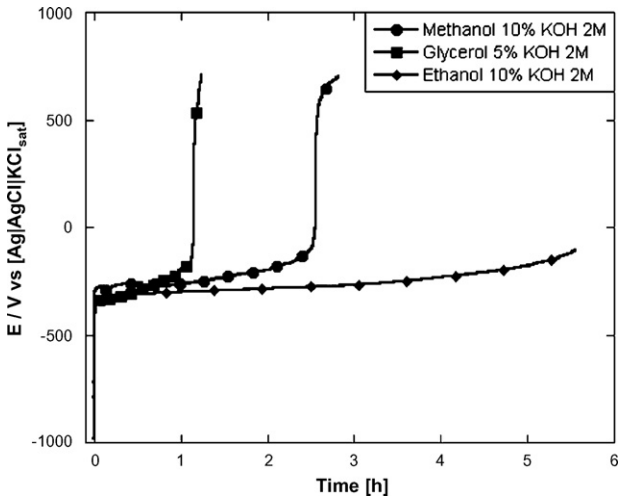

Fig. 8. Chronopotentiometric traces of methanol (10 wt.%), ethanol (10 wt.%) and glycerol (5 wt.%) oxidation on a *Pd*/*MWCNT* electrode at 3.46 $mA\,cm^{-2}$ in 2 M KOH solution.

As put in evidence by the IC analysis of the chronopotentiometric solutions after 5 h and by the NMR analysis of the exhausts of passive and active DEFCs (*vide infra*), it has been possible to establish that the oxidation of ethanol on *Pd*/*MWCNT* yields selectively acetic acid, transformed into acetate ion in the alkaline media of the reaction (Eq. (1)). The increase in the response potential after 3 h might be due to several factors, which include the increasing viscosity of the solution at the electrode interphase, resulting in a slower diffusion rate of ethanol, the decreasing concentration of OH^- anions due to their consumption (see Eq. (1)) and the increasing coverage of the catalyst surface with Pd-acetyl species whose reaction with OH_{ads} is believed to generate acetic acid [2].

$$C_2H_5OH + 5OH^- \rightarrow CH_3COO^- + 4H_2O + 4e^- \qquad E^\circ -0.743\,V \quad (1)$$

Unlike ethanol, the potentials of glycerol and methanol oxidation increased rapidly with time, reaching the value of the oxygen evolution reaction only after 1 and 2 h, respectively, which is consistent with an effective electrode deterioration under the static half cell conditions.

For a rationalization of the chronopotentiometric tests, it may be useful to anticipate the results obtained from galvanostatic experiments with passive DAFCs (alcohol = methanol, ethanol, glycerol) (*vide infra)*. IC and NMR analysis of the cell exhausts showed unequivocally that ethanol was selectively converted on the *Pd*/*MWCNT* anode to acetate with no detection of intermediate species, while methanol gave carbonate via formate. In contrast, glycerol was converted to a plethora of species among which the C-C bond cleavage products glycolate, oxalate, formate and CO_3^{2-} (Scheme 1).

The lower electrochemical stability of the *Pd*/*MWCNT* electrode for the methanol oxidation as compared to ethanol oxidation can be accounted for by the formation of CO as intermediate species in the former reaction. Indeed, unlike ethanol which is selectively converted to acetate, the oxidation of methanol on *Pd*/*MWCNT* occurs with formation of CO, successively oxidized to CO_2 (detected as CO_3^{2-} in the alkaline media of the present electrochemical reactions) (*vide infra*). The oxidation of CO adsorbed on noble metals such as Pt or Pd is rather difficult to achieve at low potential due to the strong binding of this molecule to metal centers [1–4,6,38]. As a matter of fact, the poisoning of Pt-based electrocatalysts by CO is an issue of extreme relevance for the development of both DAFCs in either acidic and alkaline conditions [1–4,6,38,39] as well

as PEMFCs (proton-exchange membrane fuel cells) using reformate hydrogen. Innumerable papers on this subject have appeared in the literature [40]. A method commonly used to alleviate the dramatic overpotentials caused by the electro-oxidation of CO_{ads} is to alloy Pt with other metals such as Ru or Sn, yet all reported Pt-based catalysts undergo deactivation with time, which requires high metal loading to ensure an acceptable durability of the corresponding DMFCs.

The formation of CO_{ads} may contribute to increase the polarization of the *Pd*/*MWCNT* electrode during glycerol oxidation, but it alone can hardly account for its much faster deactivation as compared to methanol oxidation (Fig. 8). In fact, the products derived from C–C bond cleavage paths, leading to CO_{ads} constitute a minor fraction (30–40%) of the overall transformation of glycerol. Besides, current studies of glycerol oxidation with nanostructured Pd catalysts supported on Vulcan XC-72, carried out in our laboratory [41], showed an inverse trend with glycerol being a much better fuel than methanol in terms of both electrode polarization and power density produced. Therefore, other factors than CO poisoning of the Pd sites must contribute to decrease the electrochemical stability of the *Pd*/*MWCNT* electrode for glycerol oxidation. It is likely that a major contribution to the observed polarization is provided just by the MWCNT support that, under the experimental conditions of the chronopotentiometric tests (room temperature), might disfavor either the access of glycerol to the active Pd sites or the desorption of the hydroxycarboxylate products (glycerate, tartronate and glycolate). It is worth recalling, in fact, that the MWCNTs used in this work contain a significant amount of surface carboxylic acid groups; therefore the different acidity of the alcohols employed as well as the different propensity of the intermediate products to form H-bonds may well affect both the mass transfer through the catalytic layer and the product desorption.

The importance of substrate diffusion/product desorption in controlling the electro-oxidation of glycerol on the *Pd*/*MWCNT* electrode was confirmed by the plot of the anodic peak current density against the square-root of the scan rate as well as the performance of the relative active DAFC. Indeed, above 50 °C, the power density produced by the DGFC was higher than that of the DEFC and only slightly inferior to that of the DMFC (*vide infra*).

For all electrodes, the anodic peak current density for alcohol oxidation was plotted against the square-root of the scan rate (Fig. 9). As shown in Fig. 9A, a linear relationship, typical of an electrochemical reaction under diffusion control, was found for the oxidation of ethanol at scan rates lower than 350 mV s^{-1}.

Above this scan rate, the slope decreased tending to a plateau, as if the peak current density were independent of the voltage scanning frequency. Apparently, at scan rates higher than 350 mV s^{-1}, the ethanol oxidation reaction on *Pd*/*MWCNT* is limited by other factors than substrate diffusion, for example the very low density of catalytic centers due to the extremely low Pd loading (17 μg cm^{-2}) (*vide infra*) as well as the desorption rate of the acetate product.

A much narrower window of diffusion-controlled kinetics was observed for the oxidation of glycerol (Fig. 9B), the independence of the peak current density on the voltage scanning frequency being attained already at scan rates above 50 mV s^{-1}.

The $Sa_p/(V^{1/2}\,s^{-1/2})$ profile acquired for the oxidation of methanol was quite surprising (Fig. 9C). Indeed, the peak current density was found to decrease with the scan rate, even by increasing the concentration of MeOH from 10 to 20 wt.%, in an attempt of magnifying the diffusion effects. Apparently, the diffusion of MeOH across the MWCNT support is very fast but the electrocatalyst is not sufficiently active and the peak current density decreases by increasing the scan rate. As an indirect confirmation of the role of the carbon support in controlling the substrate diffusion, we have found that the oxidation of methanol on an electrode catalyzed by nanostructured Pd particles supported on Vulcan XC-72 (same metal loading as in *Pd*/*MWCNT*) is diffusion-controlled in the range of scan rates from 50 to 500 mV s^{-1} [42].

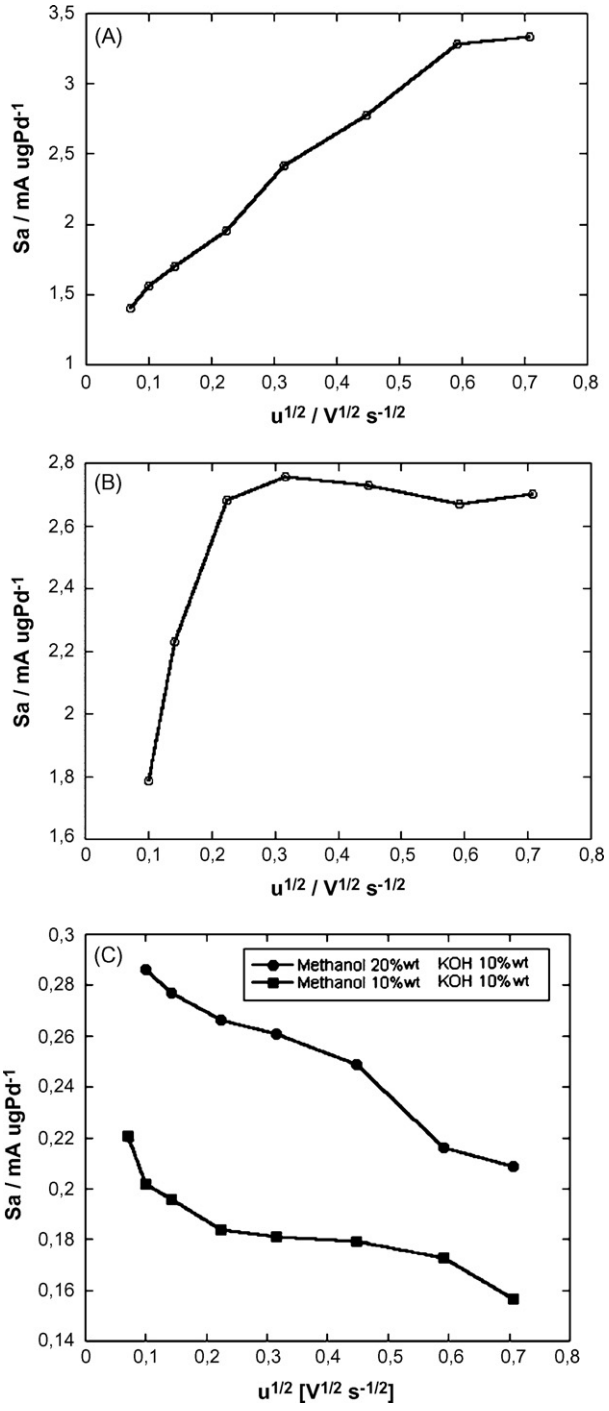

Fig. 9. Plots of the anodic peak current density against the square-root of the scan rate for the oxidation on the *Pd*/*MWCNT* electrode of (A) ethanol; (B) glycerol; and (C) methanol (10 wt.% MeOH and 2 M KOH; 20 wt.% MeOH and 2 M KOH).

3.3. DAFCs fuelled with methanol, ethanol or glycerol containing Pd/MWCNT-catalyzed anodes

3.3.1. Passive (oxygen-breathing) systems

The MEAs for the passive monoplanar DAFCs (Fig. 1) were realized as described in Section 2.4.3 with the anode catalyzed by *Pd*/*MWCNT* (0.7 mg cm^{-2} Pd), a Fe-Co Hypermec™ K-14 cathode and a Tokuyama A-006 membrane.

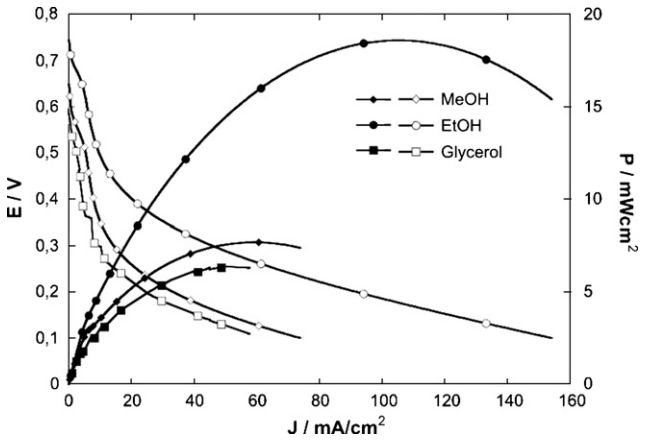

Fig. 10. Polarization and power density curves provided by oxygen-breathing DAFCs fuelled with 2 M KOH solutions of methanol (10 wt.%), ethanol (10 wt.%) and glycerol (5 wt.%) at 20–22 °C.

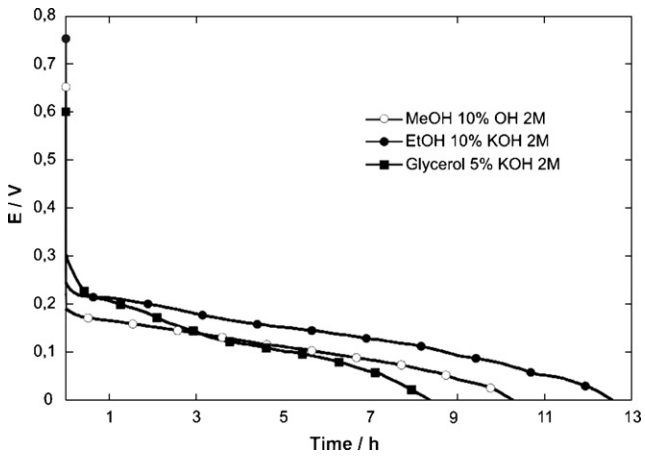

Fig. 11. Galvanostatic traces of DAFCs fuelled with methanol, ethanol or glycerol oxidation at 102 mA.

The polarization and power density curves obtained with methanol, ethanol and glycerol in 2 M KOH solution at room temperature (20–22 °C) are reported in Fig. 10. From a perusal of this figure, one may readily realize that the cell fuelled with ethanol shows the highest OCV (0.74 V) and peak power density (18.4 mW cm^{-2} at 0.2 V). To the best of our knowledge, no report has ever appeared in the relevant literature describing a passive DEFC equipped with an anion-exchange membrane.

Just to better appreciate the result obtained with the present DEFC, a comparable power density (27 mW cm^{-2} at 25 °C) has been recently obtained with an *alkaline fuel cell* (AFC) with a 3 M KOH solution as electrolyte and an anode catalyzed with 1 mg cm^{-2} of Pt-black [43]. By the way, this AFC was reported to be selective for the transformation of ethanol into acetaldehyde.

The lower performances of the DMFC and DGFC as compared to the DEFC are in line with the corresponding chronopotentiometric experiments (Fig. 8) for which a tentative explanation has been given above. The formation of carbonate upon oxidation of MeOH and to a lesser extent of glycerol, which may lead to membrane carbonatation, does not seem to account for the lower performances of the DMFC and DGFC. In fact, the power densities obtained with the three fuels investigated did not appreciably vary by using MEAs where the membrane was either in the OH^--form or in the CO_3^{2-}-form.

While no comparison can made with other DGFCs for the lack of known examples, the power density provided by the DMFC (8 mW cm^{-2}) matches well the value reported by Coutanceau et al. for a DMFC fuelled with MeOH in 1 M NaOH, and equipped with an ADP-type membrane from Solvay and an anode catalyzed with 2 mg cm^{-2} of Pt–Pd nanoparticles supported on Vulcan XC-72 [6].

Galvanostatic experiments were carried out with the present DMFC, DEFC and DGFC (Fig. 1) charging the anode compartment with 40.7 mmol of MeOH, 28.3 mmol of EtOH or 6.8 mmol of glycerol, respectively. After a conditioning time of 1 h at the OCV, the circuit was closed and a constant current of 102 mA was allowed to flow until zero voltage (Fig. 11).

The DEFC continued to deliver constantly 102 mA for 12.5 h yielding 12 mmol of acetate and leaving 12 mmol of unreacted EtOH, as determined by $^{13}C\{^1H\}$ NMR spectroscopy on the cell exhausts (Fig. 12A) (see Section 2). Accordingly, ca. 4 mmol of EtOH were lost by evaporation, likely from the cathode side as cross-over alcohol. The overall DEFC reaction can be illustrated as in Eq. (2).

$$C_2H_5OH + O_2 + OH^- \rightarrow CH_3COO^- + 2H_2O \quad (2)$$

Under comparable conditions, the DMFC lasted 10.3 h yielding 3 mmol of formate and 7 mmol of carbonate, according to Eqs. (3) and (4), with 22 mmol of unreacted MeOH (Fig. 12B). The loss of substrate was therefore of ca. 8 mmol, in line with the lower boiling point of methanol and its easier permeation through the membrane as compared to ethanol.

$$CH_3OH + O_2 + OH^- \rightarrow HCOO^- + 2H_2O \quad (3)$$

$$HCOO^- + \tfrac{1}{2}O_2 + OH^- \rightarrow {CO_3}^{2-} + H_2O \quad (4)$$

The qualitative and quantitative analysis of the DGFC exhausts was complicated by the variety of products obtained (Scheme 1 and Fig. 12C).

Overall, the cell continued to provide current for 8.4 h producing 3070 coulomb and leaving 10 mmol of unreacted glycerol. In line with the high boiling point and size of the latter molecule, no appreciable loss of fuel occurred, as the products obtained accounted for the 3.8 mmol of glycerol consumed. The following product distribution was determined by NMR and IC: glycolate (4%), glycerate (27%), tartronate (23%), oxalate (15%), formate (9%), carbonate (22%).

Most importantly, all the DAFCs described above were fully regenerated (same OCV and galvanostatic performance) upon replacement of the cell exhausts with fresh 2 M KOH solutions of methanol (10 wt.%), ethanol (10 wt.%) or glycerol (5 wt.%). This procedure was repeated four times with no apparent performance decay. Therefore, we are inclined to ascribe the severe polarizations shown in Fig. 11 to the increasing viscosity of the solutions and the competitive adsorption of substrate/partial oxidation product on the catalyst surface rather than to catalyst or electrode poisoning.

3.3.2. *Active DAFCs*

The MEAs for the active monoplanar DAFCs were realized as described in Section 2.4.4 with the anode catalyzed by *Pd/MWCNT* (1 mg cm^{-2} Pd), a Fe-Co Hypermec^{TM} K-14 cathode and a Tokuyama A-006 membrane. The fuel (water solutions containing 10 wt.% methanol, 10 wt.% ethanol or 5 wt.% glycerol) was delivered to the anode at 4 mL min^{-1}, while the oxygen flow was regulated at 200 mL min^{-1}. Each cell temperature was regulated at 25, 40, 60 or 80 °C.

Fig. 13 shows the polarization and power density curves for all the DAFC investigated.

In the temperature interval from 25 to 40 °C, the performance trend exhibited by the three DAFCs was analogous to that found for the passive cells, with the DEFC being superior to both the DMFC and the DGFC. Unexpectedly, however, increasing the cell temperature to 60 °C led to a reverse order of activity with the highest power density provided by the DMFC (peak power density of 95 mW cm^{-2} at 80 °C) and the lowest peak power density provided by the DEFC (73 mW cm^{-2} at 80 °C). In particular, the latter cell was featured by

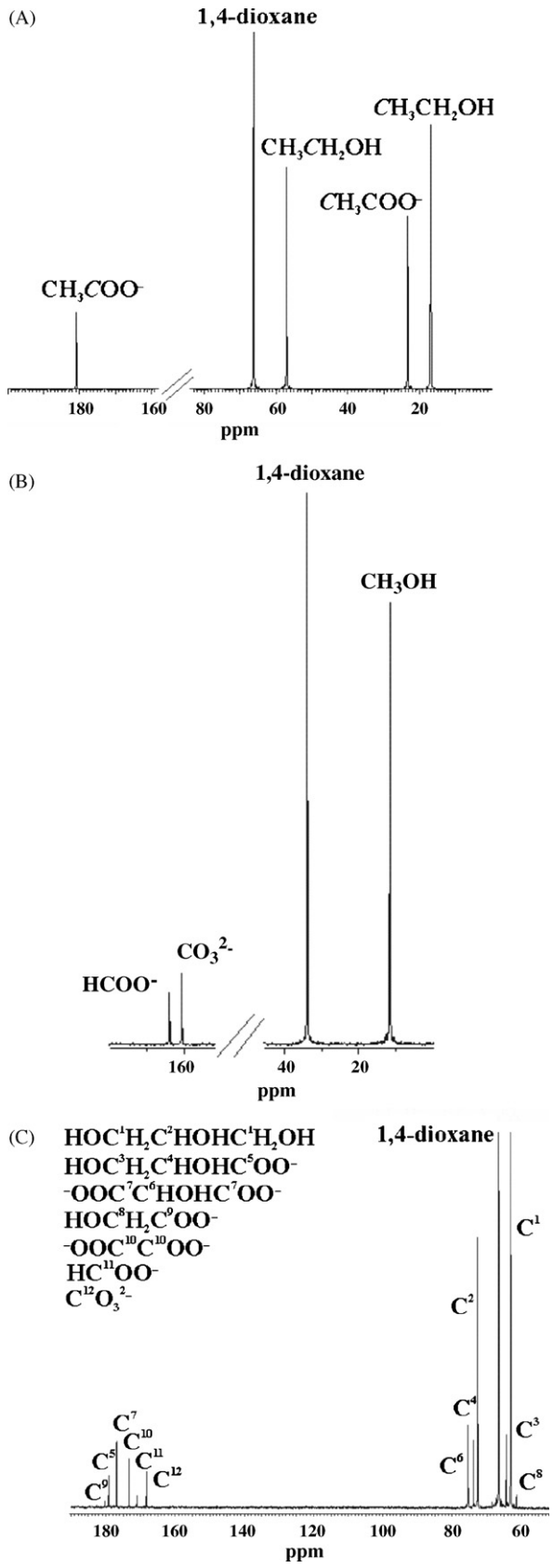

Fig. 12. $^{13}C\{^{1}H\}$ NMR spectra at room temperature of the anode solution after 12.5 h at 102 mA of (A) DEFC; (B) DMFC; and (C) DGFC.

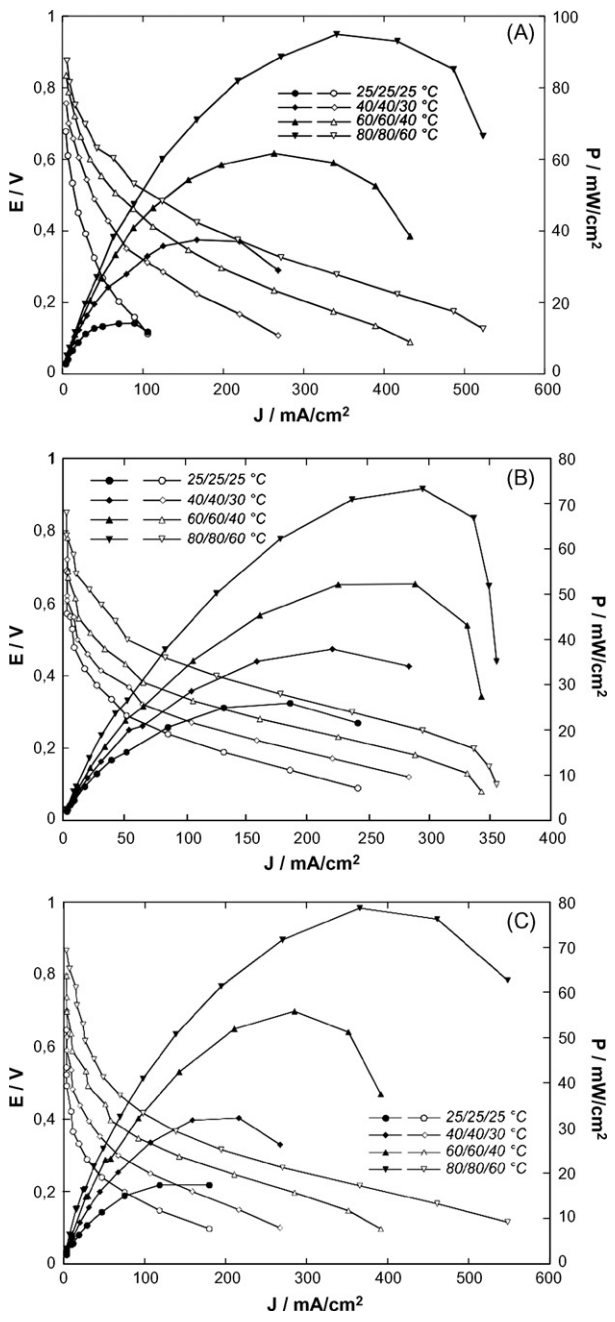

Fig. 13. Polarization and power density curves at different temperatures of active DAFC with a *Pd*/*MWCNT* anode (metal loading 1 mg cm^{-2}), fuelled with an aqueous 2 M KOH solution of (A) methanol (10 wt.%); (B) ethanol (10 wt.%); (C) glycerol (5 wt.%). Inset report the temperatures of fuel (left), cell (central), oxygen gas (right).

a sudden drop of voltage after 300 mA cm^{-2}, which is consistent with a strong contribution of the concentration polarization to the overall cell polarization. Below 300 mA cm^{-2} at 80 °C, the DEFC was competitive with the other cells. In the absence of further data, it would be hazardous to put forward any clear-cut explanation for these results. On the other hand, it is reasonable to think of a specific role of the functionalized MWCNT support in differentiating the diffusion of each substrate at high temperature. Indeed, recent studies in our laboratory have shown that ethanol is a better fuel than methanol or glycerol at any temperature from 20 to 80 °C in DAFCs identical with those described in this work except for having the anode catalyzed by nano-sized Pd particles supported on Vulcan XC-72 instead of MWCNTs [42].

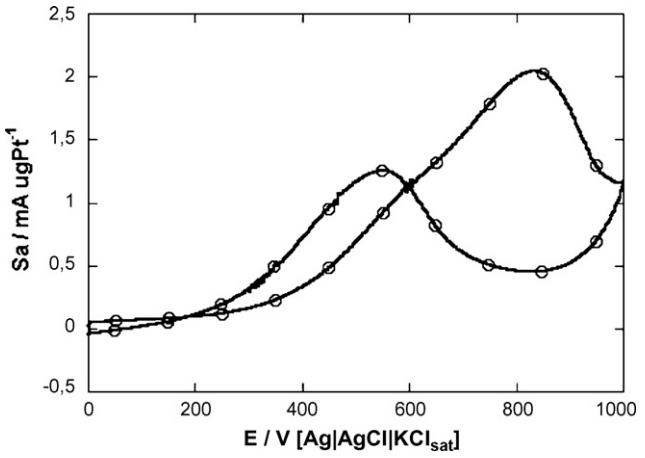

Fig. 14. Cyclic voltammograms (at the fifth cycle) of methanol oxidation on a *Pt–Ru/MWCNT* electrode in 0.5 M H_2SO_4 solution. Metal loading: 37 μg. Scan rate: 50 mV s^{-1}.

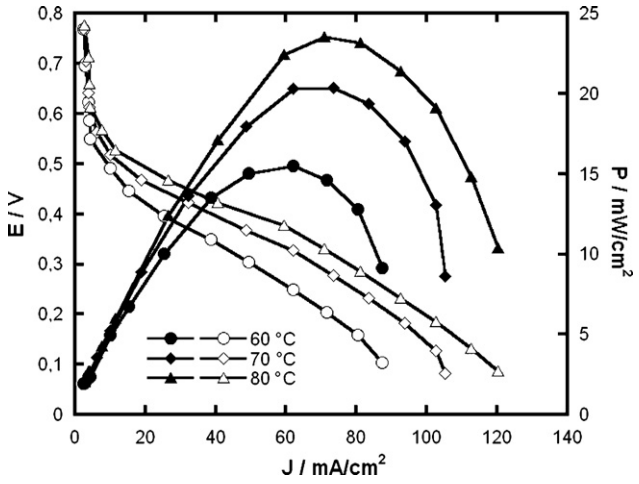

Fig. 15. Polarization and power density curves at different temperatures of an active DMFC with a *Pt–Ru/MWCNT* anode, fuelled with an aqueous 0.5 M H_2SO_4 solution of methanol (10 wt.%).

Unlike the case of the passive DAFCs for which the absence of reports in the literature has not allowed us to make a comparative study, some examples of active devices with anion-exchange membranes have been already described. Ogumi et al. have reported on active DAFCs fed with 1 M KOH solutions of various alcohols and polyalcohols, including methanol and glycerol, but not ethanol [36]. The anode and cathode catalyst were Pt–Ru/C (4 mg cm^{-2}) and Pt/C (1 mg cm^{-2}) (C = Vulcan XC-72) from E-TEK (USA), respectively, and the solid electrolyte was a Tokuyama AHA membrane. At 45 °C, the peak power densities with methanol and glycerol were 8 mW cm^{-2} at 28 mA cm^{-2} and 6 mW cm^{-2} at 27 mA cm^{-2}, respectively. Scott et al. have investigated the performance of an active DMFC using a Morgane®-ADP membrane from Solvay using Pt–Ru/C (1 mg cm^{-2}) as anode catalyst and Pt/C as cathode catalyst (both from E-TEK) [35]. At 60 °C using an oxygen flow, the highest power density was ca. 11 mW cm^{-2} at ca. 40 mA cm^{-2}. An active alkaline DEFC has been described by Hou et al. where the anode and cathode were catalyzed by commercial (Johnson-Matthey) Pt–Ru/C (2 mg cm^{-2}) and Pt/C (1 mg cm^{-2}) catalysts, respectively and the solid electrolyte was a polybenzylimidazole membrane doped with KOH, which is not a real anion-exchange membrane, however [44]. At 75 °C, a peak power density of 49 mW cm^{-2} was obtained that increased to 61 mW cm^{-2} by increasing the cell temperature to 90 °C.

Since the peak power densities provided by the present DAFCs at 80 °C range from 95 mW cm^{-2} with MeOH to 73 mW cm^{-2} with EtOH at Pd loadings of ca. 1 mg cm^{-2}, one may readily conclude that *Pd/MWCNT* exhibits unrivalled activity as anode electro-catalyst for alcohol oxidation.

3.4. Electrochemical oxidation of methanol on Pt–Ru/MWCNT in half cells and in an active DMFC with a proton-exchange membrane

Since most of the known anode electrocatalysts for DAFCs are still based on nano-sized Pt, alone or in combination with other metals, especially Pt–Ru alloys, supported on carbon blacks or CNTs [1–4,25–27,45–48], *Pt–Ru/MWCNT* electrodes were prepared and tested in both half-cell and active DMFC. Preliminary tests with ethanol and glycerol gave quite poor results and were not considered further. The limited study reported below was purposefully carried out to compare the performance of the *Pd/MWCNT* electrocatalyst in alkaline media with that of the *Pt–Ru/MWCNT* electrocatalyst in acidic media.

Fig. 14 shows the cyclic voltammogram of the methanol oxidation on a *Pt–Ru/MWCNT* electrode (Pt 24 μg cm^{-2}, Ru 13 μg cm^{-2}) in 0.5 M H_2SO_4 at a scan rate of 50 mV s^{-1}. A peak current density (J_p) of 38 mA cm^{-2} was observed at a forward anodic peak potential of 0.83 V. The onset potential of MeOH oxidation was at 0.2 V and the specific peak current density (Sa_p), relative to Pt, was 2 mA (μg Pt)$^{-1}$. The $J_{forward}/J_{backward}$ ratio of 1.4 is consistent with a modest tolerance to CO poisoning as expected for a Pt–Ru catalyst where the two metals are in a 1:1 atomic ratio [1,26]. Overall, these CV characteristics are in line with those reported in the literature for a number of Pt–Ru nanoparticles supported on carbon nanotubes [25,26,27,46].

The performance stability of the *Pt–Ru/MWCNT* electrocatalyst for methanol oxidation was investigated by chronopotentiometry. Steady state measurements were carried out by a constant current density polarization of 3.46 mA cm^{-2}. The potential of methanol oxidation increased rapidly with time, reaching the value of the oxygen evolution reaction only after 40 min, which is consistent with an effective electrode deterioration.

The MEA for the active monoplanar DMFC was realized as described in Section 2.4.4 with the anode catalyzed by *Pt–Ru/MWCNT* (metal loading: 0.70 mg cm^{-2}), the cathode catalyzed with a commercial Pt/C (30 wt.% metal) catalyst (E-TEK) (2 mg cm^{-2}) and a Nafion® 117 membrane. Methanol was delivered at 1.5 mL min^{-1}, while the oxygen flow was 200 mL min^{-1}. The cell temperature was regulated at 60, 70 and 80 °C.

Fig. 15 shows the polarization and power density curves for a cell working at 60, 70 or 80 °C. Considering the low Pt loading of the MEA in the present DMFC (0.43 mg cm^{-2} at the anode), the performance of the latter matches well those reported in the literature (from 55 to 100 mW cm^{-2} at Pt–Ru loadings of 3–4 mg cm^{-2}) for a number of DMFCs containing Pt–Ru nanoparticles supported on CNTs [45,46,47]. On the other hand, it is also apparent that the alkaline DMFC with the anode catalyzed with *Pd/MWCNT* (Fig. 13A) provides much better results in terms of both electrochemical activity and stability.

4. Conclusions

The MWCNT-supported palladium nanoparticles prepared and characterized in this work are effective catalysts for the electrooxidation in alkaline environment of methanol as well as renewable alcohols like ethanol and glycerol. The oxidation of these alcohols has been primarily investigated in half cells by a variety of electrochemical techniques, using glassy carbon electrodes. The results obtained have highlighted the excellent electrocatalytic activity of

Pd|*MWCNT* in terms of both peak current density, as high as 2800 A $(g\,Pd)^{-1}$ with glycerol, and onset oxidation potential, as low as −0.75 V vs. $Ag/AgCl/KCl_{sat}$ with ethanol. Such a remarkable electrocatalytic activity of *Pd*|*MWCNT* can be associated both to the high dispersion of the metal particles and to the intrinsic properties of the MWCNTs.

Membrane-electrode assemblies (MEA) containing a *Pd*|*MWCNT* anode, a commercial Fe-Co Hypermec™ cathode and a Tokuyama A-006 anion-exchange membrane have provided excellent results in monoplanar fuel cells. The MEA performance has been evaluated in either passive and active DAFCs fed with aqueous solutions of 10 wt.% methanol, 10 wt.% ethanol or 5 wt.% glycerol. In view of the peak power densities obtained in the temperature range from 20 to 80 °C, at Pd loadings at the anode as low as 1 mg cm^{-2}, one can safely conclude that *Pd*|*MWCNT* exhibits unrivalled activity as anode electrocatalyst for DAFCs.

Ionic chromatography and $^{13}C\{^1H\}$ NMR spectroscopy have been employed to analyze the anode exhausts of galvanostatic experiments showing that ethanol is selectively oxidized on *Pd*|*MWCNT* to acetic acid, converted to acetate ion in the alkaline media of the reaction, while methanol yields carbonate and formate. A much wider product distribution, including glycolate, glycerate, tartronate, oxalate, formate and carbonate, was obtained from the oxidation of glycerol.

A comparison with a DMFC containing a *Pt–Ru*|*MWCNT* anode catalyst has fully confirmed the superior performance of *Pd*|*MWCNT* in alkaline media.

Among the fuels investigated, ethanol is giving rise to the major interest as the relative DEFCs, either passive or active, combine excellent power outputs with superior stability with time. The oxidation of ethanol to acetic acid, isolable as potassium acetate, presages the use of *Pd*|*MWCNT* to realize alkaline direct fuel cells capable of producing selective chemicals from alcohols with concomitant release of energy.

Acknowledgments

Thanks are due to ACTA SpA, the Italian Ministry of Research (FISR project “Nanosistemi inorganici ed ibridi per lo sviluppo e l’innovazione di celle a combustibile) and the European Commission (Network of Excellence IDECAT (contract n. NMP3-CT-2005-011730) for financial support. Acta S.p.A. and Tokuyama Corporation are gratefully acknowledged for providing the cathodes and anion-exchange membranes, respectively. Jacques Teddy is grateful to the Ministère délégué à l’Enseignement Supérieur et à la Recherche for a PhD research grant.

References

[1] C. Lamy, A. Lima, V. LeRhun, F. Delime, C. Coutanceau, J.-M. Léger, J. Power Sources 105 (2002) 283.
[2] F. Viguer, S. Rousseau, C. Coutanceau, J.-M. Léger, C. Lamy, Top. Catal. 40 (2006) 111.
[3] E. Antolini, J. Power Sources 170 (2007) 1.
[4] J.S. Spendelow, A. Wieckowski, Phys. Chem. Chem. Phys. 9 (2007) 2654.
[5] K.Y. Chan, J. Ding, J. Ren, S. Cheng, K.Y. Tsang, J. Mater. Chem. 14 (2004) 505.
[6] C. Coutenceau, L. Demarconnay, C. Lamy, J.-M. Léger, J. Power Sources 156 (2005) 14.
[7] H. Igarashi, T. Fujino, Y. Zhu, H. Uchida, M. Watanabe, Phys. Chem. Chem. Phys. 3 (2001) 306.
[8] P.K. Shen, C. Xu, Electrochem. Commun. 8 (2006) 184.
[9] Z. Wang, F. Hu, P.K. Shen, Electrochem. Commun. 8 (2006) 1764.
[10] C. Xu, Z. Tian, P. Shen, S.P. Jiang, Electrochim. Acta 53 (2008) 2610.
[11] C. Xu, P.K. Shen, Y. Liu, J. Power Sources 164 (2007) 527.
[12] S.-H. Hong, M.-S. Jun, I. Mochida, S.-H. Yoon, in: P. Barbaro, C. Bianchini (Eds.), Catalysis for Sustainable Energy Production, Wiley, 2009.
[13] R. Pattabiraman, Appl. Catal. A: Gen. 153 (1997) 9.
[14] F. Hu, C. Chen, Z. Wang, G. Wei, P.K. Shen, Electrochim. Acta 52 (2006) 1087.
[15] M. Nie, H. Tang, Z. Wei, S.P. Jiang, P.K. Shen, Electrochem. Commun. 9 (2007) 2375.
[16] C. Xu, L. Cheng, P. Shen, Y. Liu, Electrochem. Commun. 9 (2007) 997.
[17] D. Yuan, C. Xu, Y. Liu, S. Tan, X. Wang, Z. Wei, P.K. Shen, Electrochem. Commun. 9 (2007) 2473.
[18] F.P. Hu, Z. Wang, Y. Li, C. Li, X. Zhang, P.K. Shen, J. Power Sources 177 (2008) 61.
[19] F. Hu, F. Ding, S. Song, P.K. Shen, J. Power Sources 163 (2006) 415.
[20] H.T. Zheng, Y. Li, S. Chen, P.K. Shen, J. Power Sources 163 (2006) 371.
[21] A. Solhy, B.F. Machado, J. Beausoleil, Y. Kihn, F. Gonçalves, M.F.R. Pereira, J.J.M. Órfão, J.L. Figueiredo, J.L. Faria, P. Serp, Carbon 46 (2008) 1194.
[22] J.-C. Hierso, PhD thesis, Université Paul Sabatier, Toulouse, 1997.
[23] Y. Sudong, Z. Xiaogang, M. Hongyu, X. Ye, J. Power Sources 175 (2008).
[24] JCPDS Card No. 00-046-1043, International Centre for Diffraction Data, Newton Square, PA, 1993.
[25] G. An, P. Yu, L. Mao, Z. Sun, Z. Liu, S. Miao, Z. Miao, K. Ding, Carbon 45 (2007) 536.
[26] J. Huang, Z. Liu, C. He, L.M. Gan, J. Phys. Chem. B 109 (2005) 16644.
[27] C. Yang, D. Wang, X. Hu, C. Dai, L. Zhang, J. Alloys Compd. 448 (2008) 109.
[28] F. Colmati Jr., W.H. Lizcano-Valbuena, G.A. Camara, E.A. Ticianelli, E.R. Gonzalez, J. Braz. Chem. Soc. 13 (2002) 474.
[29] A. Caillard, C. Coutanceau, P. Brault, J. Mathias, J.-M. Léger, J. Power Sources 162 (2006) 66.
[30] C.-C. Hu, T.-C. Wen, Electrochim. Acta 41 (1996) 1505.
[31] C.-C. Hu, T.-C. Wen, Electrochim. Acta 40 (1995) 495.
[32] M. Grden, M. Łukaszewski, G. Jerkiewicz, A. Czerwinski, Electrochim. Acta 53 (2008) 7583.
[33] J.P. Singh, X.G. Zhang, Hu-lin Li, A Singh, R.N. Singh, Int. J. Electrochem. Sci. 3 (2008) 416.
[34] V.M. Barragán, A. Heinzel, J. Power Sources 104 (2002) 66.
[35] K. Scott, E. Yu, G. Vlachogiannopoulos, M. Shivare, N. Duteanu, J. Power Sources 175 (2008) 452.
[36] K. Matsuoka, Y. Iriyama, T. Abe, M. Matsuoka, Z. Ogumi, J. Power Sources 150 (2005) 27.
[37] A.E. Bolzán, A.J. Arvia, J. Electroanal. Chem. 157 (1992) 247.
[38] L. Demarconnay, S. Brimaud, C. Coutanceau, J.-M. Léger, J. Electroanal. Chem. 601 (2007) 169.
[39] K. Matsuoka, Y. Iriyama, T. Abe, M. Matsuoka, Z. Ogumi, Electrochim. Acta 51 (2005) 1085.
[40] R. Borup, J. Meyers, B. Pivovar, Y.S. Kim, R. Mukundan, N. Garland, D. Myers, M. Wilson, F. Garzon, D. Wood, P. Zelenay, K. More, K. Stroh, T. Zawodzinski, J. Boncella, J.E. McGrath, M. Inaba, K. Miyatake, M. Hori, K. Ota, Z. Ogumi, S. Miyata, A. Nishikata, Z. Siroma, Y. Uchimoto, K. Yasuda, K.-C. Kimijima, N. Iwashita, Chem. Rev. 107 (2007) 3904.
[41] V. Bambagioni, C. Bianchini, J. Filippi, W. Oberhauser, A. Marchionni, F. Vizza, R. Psaro, L. Sordelli, M.L. Foresti, M. Innocenti, ChemSusChem 2 (2009) 99.
[42] C. Bianchini, F. Vizza, unpublished result.
[43] A. Verma, S. Basu, J. Power Sources 145 (2005) 282.
[44] H. Hou, G. Sun, R. He, Z. Wu, B. Sun, J. Power Sources 182 (2008) 95.
[45] K.-T. Jeng, C.-C. Chien, N.-Y. Hsu, S.-C. Yen, S.-D. Chiou, S.-H. Lin, W.-M. Huang, J. Power Sources 160 (2006) 97.
[46] Z. Liu, X.Y. Ling, B. Guo, L. Hong, J.Y. Lee, J. Power Sources 167 (2007) 272.
[47] K.-T. Jeng, C.-C. Chien, N.-Y. Hsu, W.-M. Huang, S.-D. Chiou, S.-H. Lin, J. Power Sources 164 (2007) 33.
[48] C.-C. Chien, K.-T. Jeng, Mat. Chem. Phys. 99 (2006) 80.